Similarities between Insect Swarms and Isothermal Globular Clusters

Dan Gorbonos and Nir S. Gov*
Department of Chemical Physics, The Weizmann Institute of Science, P.O. Box 26, Rehovot, Israel 76100

Kasper van der Vaart, Michael Sinhuber, and Nicholas T. Ouellette
Department of Civil and Environmental Engineering, Stanford University, Stanford, California 94305, USA

James G. Puckett
Department of Physics, Gettysburg College, Gettsyburg, Pennsylvania 17325, USA

Andrew M. Reynolds
Rothamsted Research, Harpenden, AL5 2JQ, UK

Previous work has suggested that disordered swarms of flying insects can be well modeled as self-gravitating systems, as long as the "gravitational" interaction is adaptive. Motivated by this work we compare the predictions of the classic, mean-field King model for isothermal globular clusters to observations of insect swarms. Detailed numerical simulations of regular and adaptive gravity allow us to expose the features of the swarms' density and velocity profiles that are due to long-range interactions, and are captured by the King model phenomenology, and those that are due to adaptivity and short-range repulsion. Our results provide further support for adaptive gravity as a model for swarms.

I. INTRODUCTION

Insect swarms are a canonical example of collective animal behavior [1, 2], displaying group-level cohesion and stability even in the presence of environmental noise [3–8]. But while in many other forms of collective animal motion, such as flocking, schooling, and herding [2], the movement of individuals is coordinated, swarms are distinguished by their lack of globally aligned motion and the swarm state is not described by any order parameter.

It is thought that many swarming insect species such as *Chironomus riparius*, the midge species we consider here, interact predominantly via long-range acoustic sensing [9]. Indeed, a theoretical model that assumes that midges accelerate toward the sounds produced by other individuals has produced nontrivial results that are in good agreement with empirical observations [10, 11]. The acoustic field produced by flying insects has a monopole component whose intensity falls off according to an inverse-square law [12], a scaling that is similar to the way the gravitational pull between objects falls off with distance. Dipole and other higher-order multipole components decay more rapidly, and are thus weaker than the monopole component. It is therefore tempting to speculate, as Okubo [3] and then Gorbonos *et al.* [10] did, that midge swarms are analogous to N-body self-gravitating systems, where cohesion originates from the gravitational pull between the bodies compromising the system. A key contribution from ref. [10] was to incorporate the adaptive gain of typical biological sensors, which leads to results that are different from Newtonian gravitation but are in good agreement with empirical measurements of swarms.

This adaptive-gravity model was shown in ref. [10] to capture many global features of midge swarms. For example, it correctly reproduces the linear radial dependence of the mean acceleration of midges towards the swarm center, the scaling of this acceleration with the swarm size, and the virial-like relation between the mean kinetic and potential energies of the whole swarm.

The analogy between swarms and self-gravitating systems is further appealing because it is well known that gravity can produce complex dynamical behavior from simple interactions—just as is thought to be the case for collective animal behavior [13]. Thus, by making a link between these two distinct systems, we can draw on the intuition built up from studying gravity to gain insight into collective animal behavior.

In this paper, we examine this analogy more closely by studying the spatial variation of the number density and the velocity of individuals. We compare to the classic King model for the mass distribution in isothermal globular clusters [14] (see appendix A). Although we find some similarities with the observed swarms, there are also significant differences. These discrepancies reveal the limitations of a pure gravitational model for swarms. Furthermore, we aim to explore which of the observed global features of the midge swarm arise from the long-range nature of the interactions and which depend also on the property of adaptivity. Long-range interactions are of course a feature of regular gravity, and therefore also appear in globular clusters, which are well described by the King model. We would then expect that features that are crucially dependent on adaptivity, which is *not* present in regular gravity, will be missing from a King-model description of the swarm. We find that the addi-

* nir.gov@weizmann.ac.il

tion of adaptivity, which we can introduce only using numerical simulations, together with short-range repulsion produces mass distributions and dynamics that capture all the main features of the midge swarm data. Thus, our results provide significant further support for adaptive gravity as a model for the swarm behavior.

II. DENSITY PROFILES

II.1. Density profiles: King's model and midge swarms

We begin by considering the mass distributions predicted for regular gravity (such as in globular clusters) by the original King model. This model has been well studied previously. Chavanis *et al.* [15], for example, described the solution space for globular clusters by fixing the cluster mass and varying the other system parameters, such as temperature, cluster radius, energy, and so forth. To adapt this model for swarms, we use a fixed inverse temperature β, which describes isothermal globular clusters. In addition to being simple to implement (see appendix A), this choice is motivated by the observation that swarms of different sizes empirically display roughly the same amount of kinetic energy per midge [16, 17]. For large globular clusters, a King model with fixed temperature gives a roughly constant kinetic energy per particle (independent of system size (Fig. 4)). With this assumption, we compute the density profiles predicted by the King model (Fig. 1(a,b)), using Eqs. A15 and A16. Note that for easier comparison between the different models, we plot the density profiles for all the models in Fig. 1, and the corresponding quantitative measures in Fig. 2.

The King model predicts two distinct branches of solutions, which are clearly observed when we plot quantitative measures of the distributions such as the total mass M (Fig. 2(a), where we assume that all midges have the same mass), the density at the center ρ_0 (Fig. 2(b)), and the kurtosis (Fig. 2(c)) as functions of the overall swarm size R_s. Here, R_s is defined as the mean distance of a midge from the center of mass of the swarm: $R_s \equiv \int_0^\infty r^3\rho(r)dr / \int_0^\infty r^2\rho(r)dr$, where $\rho(r)$ is the density profile. The two branches are termed "stable" and "unstable" (shown in blue and red, respectively, in Fig. 2(a-c)), and are distinguished by the sign of the heat capacity (positive or negative, respectively) of the cluster in the canonical ensemble [15]. It is found empirically that globular clusters reside on the unstable branch [15], presumably due to the strong destabilizing effects of "slingshots"—that is, anomalously high acceleration events that arise due to close encounters.

In Fig. 1(c,d) we plot the empirical density profiles measured for laboratory midge swarms. Details of the laboratory setup and measurement protocols are given in refs. [4] and [18]. The primary difference between the data in Fig. 1(c) and (d) is that the swarms in (c) were observed in a cubical laboratory enclosure measuring 91 cm on a side, while the enclosure for the swarms in (d) measured 122 cm on a side.

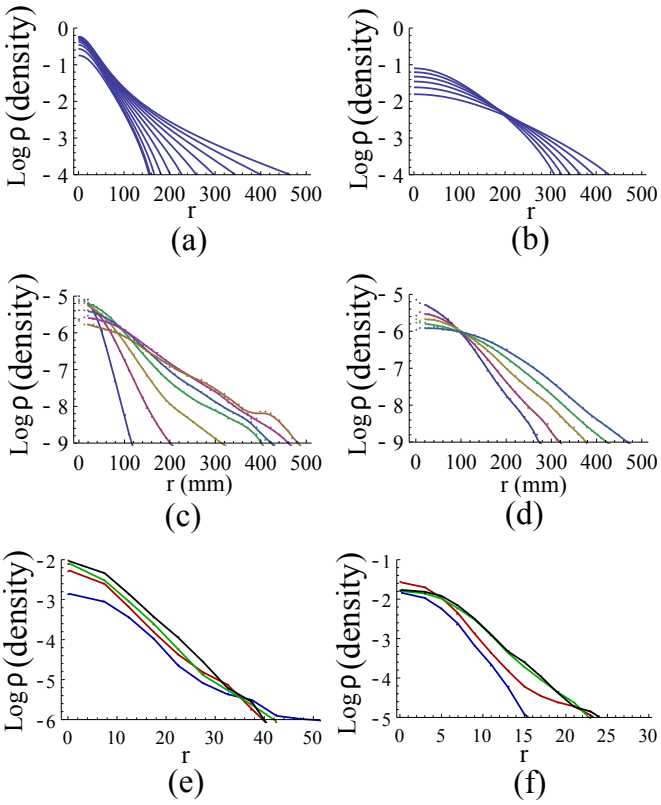

FIG. 1. (a, b) Two families of density profiles computed from the King model (Eqs. A15-A16) for different initial conditions, with shapes that are qualitatively similar to results from real swarms (c, d). (a) corresponds to the unstable branch, and (b) to the stable branch (see the discussion in the text). (c, d) Two families of density profiles measured in real swarms in two different laboratory setups (see text). (e) Density profiles of simulated swarms using the adaptive gravity model. Simulations were run using $N = 12$ and $R_s = 16.2$ (blue); $N = 24$ and $R_s = 11.8$ (red); $N = 32$ and $R_s = 11.5$ (green); and $N = 48$ and $R_s = 12$ (black). (f) Density profiles of simulated swarms including adaptivity and short-range repulsion. Simulations were run using $N = 12$ and $R_s = 6$ (blue); $N = 24$ and $R_s = 6.7$ (red); $N = 32$ and $R_s = 8.2$ (green); and $N = 48$ and $R_s = 8.1$ (black).

Qualitatively, the density profiles from the swarms are similar in many aspects to those computed from the King model, though the agreement is not exact. To illuminate these similarities and differences further, we computed the same distribution measures for the swarms as for the King model, shown in Fig. 2(d-f). The density at the center of the midge swarm (ρ_0) was obtained in Figs. 2(e,h,k) by fitting a Gaussian to the density profile near the center of mass. We see in Fig. 2e that ρ_0 slightly decreases with increasing swarm size, which qualitatively fits the stable branch of the King model (where this decrease is much steeper). The total number of midges (as a proxy for the total mass) increases slowly with the swarm ra-

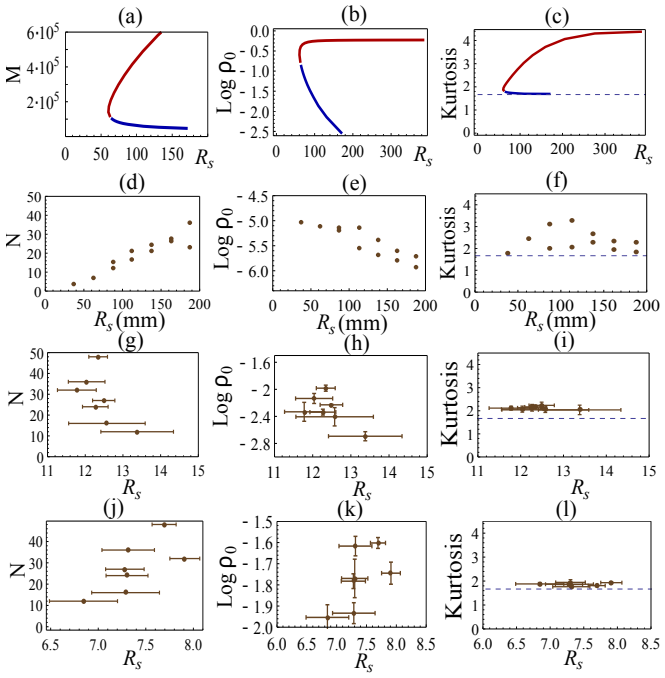

FIG. 2. (a-c) Total mass M (a), density at the center ρ_0 (b), and kurtosis (c) as a function of the swarm size R_s for a series of King model solutions. The blue line corresponds to the stable branch in the canonical ensemble and the red one to the unstable one. The kurtosis of a Gaussian distribution in three dimensions, 5/3, is denoted by the horizontal dashed line. (d-f) The same quantities computed from the measured data for real swarms. (g-i) The same quantities computed for simulated swarms with adaptivity. (j-l) The same quantities computed for simulated swarms with adaptivity and short-range repulsion.

dius, a feature exhibited by the unstable branch of the King model (the stable branch has the opposite relation).

The kurtosis of the midge swarms falls in a range of values between the King model branches, and is significantly larger (i.e., the swarms have heavier tails than they would if they were Gaussian) than the density profiles along the King model stable branch (which are very close to Gaussian). Note that the kurtosis is a standard measure to quantify simple but non-Gaussian distribution shapes (as long as they are monotonically decreasing functions, as shown in Fig. 1). Thus, it provides an interpretable way of comparing the different models, and highlights discrepancies between the midge swarms and the King model behavior.

II.2. Density profiles: modified gravity models

To attempt to reconcile the model predictions with the empirical results for real swarms, we consider two modifications to normal Newtonian gravity. First, since particles in the simulations have a strong tendency to develop anomalously high accelerations due to slingshots and thus to evaporate from the cluster, it is common to include a softening parameter ϵ (with units of length) to the gravitational force [19], so that

$$\vec{F}^i_{\epsilon,g} = C\sum_j \hat{r}_{ij}\frac{1}{|\vec{r}_i-\vec{r}_j|^2+\epsilon^2}, \tag{1}$$

where C is a constant with units of (force $\times$ length^2), $\vec{r}_i$ is the position vector for midge i, and $\hat{r}_{ij}$ is the unit vector pointing from midge i to midge j. This "epsilon"-gravity modifies the force at short distances, up to $|\vec{r}_i-\vec{r}_j| = O(\epsilon)$. We chose a value of $\epsilon=\sqrt{15}\simeq 3.87$, so that it is smaller than the mean swarm size R_s (Figs.1,15) but is still effective in preventing slingshots and maintaining a stable swarm.

In addition, we simulated our previously introduced adaptive-gravity model [10]. In this case, the effective force felt by midge i due to midge j is given by

$$\vec{F}^i_{\rm eff} = C\sum_j \frac{\hat{r}_{ij}}{|\vec{r}_i-\vec{r}_j|^2+\epsilon^2}\frac{R_{\rm ad}^{-2}}{R_{\rm ad}^{-2}+\sum_k\left(|\vec{r}_i-\vec{r}_k|^2+\epsilon^2\right)^{-1}} \tag{2}$$

The logic underlying this model is that the strength of the signal received by each midge should be renormalized by the total buzzing noise due to all the other midges, to mimic the typical adaptive gain of biosensors [20]. We define a length scale, $R_{\rm ad}$, over which this adaptivity occurs, and when $r_{ij}\gg\sqrt{N}R_{\rm ad}$, such that the distance between a pair of midges is much larger than the adaptive range, the model reduces to epsilon-gravity (which itself reduces to Newtonian gravity when $\epsilon=0$). Within the range of adaptivity, where the midges are close to each other compared to $R_{\rm ad}$, the term $R_{\rm ad}^{-2}$ is negligible in the denominator of the second factor in Eq. 2, and we see that the vectorial sum of the first factor is simply divided by the scalar sum in the second factor. This gives rise to what we term "perfect adaptivity," where the response does not depend on the absolute intensity of the background signal.

Finally, we also simulated the adaptive-gravity model with an additional short-range repulsion between the midges. This effect was empirically observed and measured in real swarms [21], and was implemented in an earlier simulation scheme [10]. This type of effective interaction arises due to midges avoiding collisions while flying. Here we use a repulsive force with a cutoff to capture this effect, given by

$$\vec{F}^i_{\rm rep} = \begin{cases} C\sum_j\left(\frac{1}{L_c^2}-\frac{1}{|\vec{r}_i-\vec{r}_j|^2}\right)\hat{r}_{ij} & |\vec{r}_i-\vec{r}_j|<L_c \\ 0 & |\vec{r}_i-\vec{r}_j|\geq L_c \end{cases} \tag{3}$$

where we take $L_c\approx 0.2\,R_{\rm ad}$. We chose this value as it was the minimal value for L_c that produced a noticeable effect on the qualitative features of the swarms, as compared with those without repulsion (see below). Larger values of L_c would make the repulsion force dominant in small, finite-size swarms, and we wanted to stay in the regime where the long-range gravity-like interactions

play the dominant role for the large-scale organization of the swarm. In the simulations we worked in the regime where $R_s/L_c \sim 4$, which is within the range observed in the experiments $R_s/L_c \sim 4-16$ [21].

With these interaction laws, we considered several different swarm sizes R_s, as defined above. We used $R_{\rm ad} = 10 \approx R_s$, placing us in the regime where adaptivity affects the vast majority of the midges in the swarm. Unlike for regular gravity, where we can use the coarse-grained King model, for adaptive-gravity we do not have at present an equivalent coarse-grained description. Therefore, to explore the spatial distribution of mass in the adaptive gravity model we turned to numerical simulations. We used a scheme for performing N-body dynamics originally developed by Aarseth (see Appendix 4.B of [22]), which allows for accurate numerical integration using fourth-order equations of motion. A complete description of the numerical method is given in ref. [19]. The acceleration of each mass in the simulation is computed by the direct summation of the forces due to the other $N-1$ bodies following the form of the force law. The scheme was designed to work efficiently for up to $N = 50$, well within the range of typical midge swarms [4, 18]. For further details about the simulation see the appendices B, F and G. Initially, particles were placed randomly in a simulation box of varying side lengths, in order to control the kinetic energy of the system. This was achieved (except for the epsilon-gravity system; see below) by varying the initial conditions of the simulations until the kinetic energy per particle was within 10% of the desired value in the long-time limit (Fig. 13). The initial velocities were zero, but under the influence of the forces the particles accelerated and eventually reached a quasi-stationary state (Figs. 5-7) that exhibits the distinct non-Gaussian velocity statistics (Fig. 8) observed in real swarms [4]. Note that we do not include explicit noise in the simulations, and the trajectories become ergodic due to the natural tendency of N-body gravitating systems to be chaotic.

We now compare the same quantitative features of the density profiles computed from the numerical simulations to those from the King model and the empirical swarm measurements. Note that the theoretical calculations of the King model and the simulations are done in arbitrary units of length, while the experimental measurements have an inherent length scale (Figs.1, 2). Wherever possible we normalized the axes to become dimensionless (such as in Figs.3,10,11), but it is not always obvious how to do so.

We start with the epsilon-gravity interaction (Eq. (1), using $\epsilon = 3.8$, which was much smaller than the swarm size R_s; Fig. 15). Not surprisingly, some measures (Fig. 15(b,c)) seem to agree well with the stable branch of the King model (Fig. 2a-c), since close-encounter slingshots are greatly suppressed by the softened gravity. Other similarities include a decrease in the size R_s and sharp decrease in ρ_0 for larger swarms.

Comparing to real midge swarms, we find that the decrease in ρ_0 for larger swarms in epsilon-gravity (Fig. 15c) is qualitatively similar, though somewhat stronger (Fig. 2e). This similarity suggests that this feature arises from the long-range character of the interactions between the midges, and that adaptivity only acts to weaken it (see below). The epsilon-gravity force law does not agree very well with another observed feature of the midge swarms (Fig. 2(d)), where the size increases with the number of particles. Note that for epsilon-gravity, we were not able to keep the kinetic energy per particle constant when changing the overall number of particles in the swarm (Fig. 14).

Figures 1(e) and 2(g-i) show the results from adaptive-gravity simulations (Eq. (2), using $R_{ad} = 10$). Note that the swarms cover a much smaller range of sizes (R_s), compared to the real (Figs. 1(c,d) and 2(d-f)) or epsilon-gravity swarms (Fig. 15). This is due to the sharp increase in the density at the center when the number of particles increases combined with the fixed kinetic energy per particle, thereby maintaining a roughly constant R_s. We find that ρ_0 decreases with increasing R_s, similar to the observations in real swarms (as well as epsilon-gravity and the stable branch of the King model). The kurtosis is similar to the values seen in the real swarms. However, just as for epsilon-gravity and the stable branch of the King model, the biggest discrepancy with the real swarms is the relation between the number of particles (midges) and R_s, which we find in the simulations to be a decreasing function (Fig. 2(g)) even though it is increasing in real swarms (Fig. 2(d)).

We therefore also tested the addition of a short-range repulsion (Eq. 3) to the adaptive-gravity simulation (Figs. 1(f) and 2(j-l)). This additional ingredient makes ρ_0 roughly independent of R_s while not changing the kurtosis significantly. Both measures are in reasonable agreement with the real swarm data, considering the small range of swarm sizes in the simulations. The primary change as a result of the short-range repulsion is the appearance of an overall increasing relation between the number of particles and swarm size (Fig. 2(j)). This feature, which is observed in the real swarms (Fig. 2(d)), is absent from all the simulations that contain only long-range attractive interactions. This model therefore captures qualitatively all the main features of the density profiles of the midge swarms.

These results allow us to clearly delineate the properties of the midge swarm that are due to the long-range (adaptive) gravity interactions, namely the large kurtosis (heavy tails) and a slow decrease of the density at the swarm center for increasing swarm sizes. The short-range repulsion is responsible for inflating the size (R_s) of swarms with increasing number of midges, which is counter to the behavior of purely long-range interactions (both epsilon and adaptive gravity).

III. VELOCITY PROFILES

So far we have considered the spatial density distribution of the swarm. We now turn to the spatial distribution of the velocities of the particles in the swarm, as another way to distinguish between the different models and compare to the observations from real swarms. We therefore computed the average speed of midges as a function of the distance r away from the center of mass of the swarm using the dataset from the larger midge enclosure [18]. As shown in Fig. 3(a), these speeds are essentially independent of position (as also noted in ref. [17]). Thus, the mean kinetic energy of a midge is also statistically uniform in space (Fig. 11a).

The simulated speed profile for epsilon-gravity is shown in Fig. 3b. We see that the velocity decreases rapidly with increasing radius from the swarm center, in good agreement with the profiles calculated from the King model but contrary to the data for real swarms. By contrast, the velocity profile computed using adaptive-gravity (Fig. 3(c)) is rather flat, with a small increase of speed for small r, presumably because the potential is too strongly softened in the swarm center. The velocity profile becomes even smoother when short-range repulsion is included (Fig. 3(d)), and is similar to the empirical results for real swarms. We find similar results for the standard deviation of the speed (Fig. 11).

The uniformity of the velocity profile across the swarm (Figs. 3, 11) serves as strong support for the adaptive-gravity model. Note that the midges do not move at constant *instantaneous* speed when flying through the swarm, and that the global velocity distribution has long (nearly exponential) tails (see [4] and Fig. 8), so it is not obvious *a priori* that there would not be some radial dependence in the local velocity distribution. Therefore, the novel observation of a flat velocity distribution (shown in Figs. 3a, 11a) in midge swarms is a challenge that must be met by any theoretical model. We demonstrate that this property does not arise in the simplest gravitational model (King model), and so it is not a consequence of long-range interactions alone. The additional property of adaptivity, however, recovers this characteristic, and we therefore view this as strong support for this model.

Finally, we considered the relation between mean acceleration and speed for swarms of different sizes (Fig. 10) [17]. We find that epsilon-gravity fails to reproduce the observed collapse of the curves for all swarm sizes, while the adaptive gravity captures this relation extremely well. This agreement gives added support to the adaptive-gravity model. It demonstrates that this model accounts for this observation, and there is no need for additional (velocity-dependent) interactions [17].

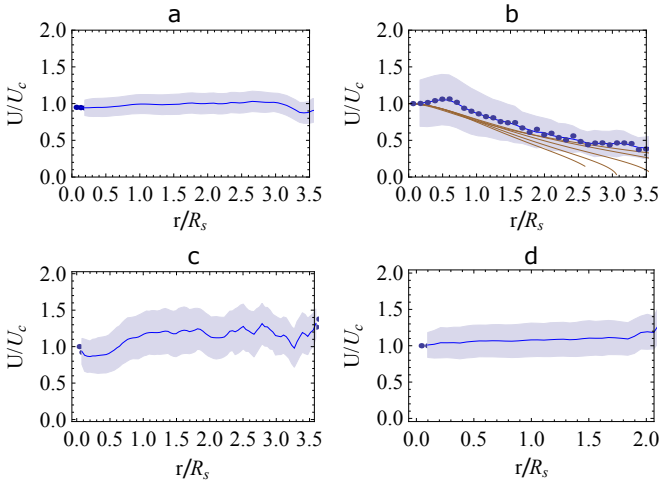

FIG. 3. Mean speed as a function distance from the center of the swarm, normalized by the speed at the center. Data are shown for (a) real laboratory swarms, (b) epsilon-gravity, (c) adaptive gravity, and (d) adaptive gravity with short-range repulsion. The brown curves in (b) correspond to a family of King model solutions (Fig. 1a,b), computed numerically according to Eq. (A23). In (d), we truncated the plot at $r \sim 2\,R_s$ since outside this radius the particles are not part of the cohesive region (i.e., the swarm) (see Fig. 12).

IV. CONCLUSION

Taken together, our results provide further evidence that the interactions in insect swarms are well described by the adaptive-gravity framework, together with a short-range repulsion. This highlights that two key ingredients—long-range interactions and adaptivity—are essential. This model naturally captures many of the unusual properties of swarms, some of which have surprising similarities to globular clusters. Adaptivity, however, also induces additional effects. When the binding to the swarm is adaptive, the forces on one midge due to the other midges are not additive, and as a consequence the sum of the forces felt by all of the midge need not vanish, as it must for Newtonian gravity [10]. The center of mass of the swarm can therefore experience accelerations [23]. Such fluctuations have the potential to change fundamentally the characteristics of individual flight patterns; for example, Reynolds and Ouellette [23] showed that center of mass fluctuations allow for the emergence of Lévy flight patterns. Centre-of-mass movements may also help to stabilize insect swarms against environmental perturbations [24].

These results suggest that it may be fruitful in the future to consider modifications of the interactions within the King model as a general framework for describing the behavior of active systems with long-range interactions, whatever their form. The proper analytical treatment of a King model augmented with an adaptive-gravity interaction law remains as a challenge for future studies. Finally, future work on swarm modeling in partic-

ular should explore the effects of adding self-propulsion and stochasticity (noise), both of which are absent from the current models but certainly present for real insects. This kind of more realistic description of the motion of individual midges may also be required for the theory to describe the response of the midge swarm to external perturbations [7, 8], and in particular the dynamics of this response.

ACKNOWLEDGMENTS

We thank Tsvi Piran, Sverre Aarseth, and Tal Alexander for useful discussions. The research at Stanford was sponsored by the Army Research Laboratory and accomplished under grant no. W911NF-16-1-0185. The views and conclusions in this document are those of the authors and should not be interpreted as representing the official policies, either expressed or implied, of the Army Research Laboratory or the U.S. government. K.v.V. acknowledges support from an Early Postdoc Mobility fellowship from the Swiss National Science Foundation, and M.S. acknowledges support from the Deutsche Forschungsgemeinschaft under grant no. 396632606. The work at Rothamsted forms part of the Smart Crop Protection (SCP) strategic programme (BBS/OS/CP/000001) funded through the Biotechnology and Biological Sciences Research Council's Industrial Strategy Challenge Fund.

Appendix A: The King Model

Most globular clusters are well-fit by the King model [25], as it captures their basic structure and main observed features [26]. This model is one of a series of models that assume a Maxwell—Boltzmann distribution of the velocities, although it is well-known that a self-gravitating system cannot actually be in thermodynamic equilibrium. This fact is a result of the long-range nature of the interactions and the Boltzmann entropy which has no maximal value in an unbounded domain. Therefore, self-gravitating systems, as part of their out-of-equilibrium nature, have a strong tendency to evaporate over time. Since evaporation is a slow process, the system can be considered to be in a quasi-stationary state for times that are much shorter than the evaporation time, and the Maxwell-–Boltzmann distribution can therefore serve as a good approximation.

In order to write a quasi-stationary expression for the distribution $f(\vec{r},\vec{v})$ (that is, as a function of position and velocity but not of time) we start from the collisionless Boltzmann equation:

$$\vec{v}\cdot\nabla f = \nabla V\cdot\frac{\partial f}{\partial \vec{v}}, \tag{A1}$$

where $V = V(r)$ is a spherically symmetric gravitational potential. The density is defined by

$$\rho = \int f d^3\vec{v}, \tag{A2}$$

and it determines the gravitational potential through the Poisson equation

$$\triangle V = 4\,\pi\,C\,\rho, \tag{A3}$$

where C is a constant with dimensions of $mass\cdot length^3/time^2$ which for the gravitational force is the gravitational constant. A simple solution to this set of equations ((A1) and (A3)) is given by the Maxwell-–Boltzmann distribution with a singular power-law behavior in the spatial part:

$$f(\vec{r},\vec{v}) \sim \frac{e^{-\frac{\beta\,\vec{v}^2}{2}}}{r^2}, \tag{A4}$$

where β is a positive constant which is identified with the inverse temperature.

This solution is singular at the origin, unbounded and has infinite mass since

$$M(r) \propto r. \tag{A5}$$

The singularity at the origin can be fixed by introducing regular boundary conditions:

$$V(0) = const, \quad V'(0) = 0, \tag{A6}$$

but this does not fix the asymptotic behavior. Numerical solutions of equations ((A1) and (A3)) with boundary conditions (A6) are solutions of isothermal spheres (since β is constant). Far from the center at $r \gg (C\,\rho(0)\,\beta)^{-\frac{1}{2}}$ the isothermal sphere solutions approach the singular solution (A4). Although the solution is not singular at the center, it is still unbounded and has infinite mass (see for instance [27], p. 480-484).

The steady-state mass distribution that solves the Poisson-Boltzmann equations is singular, proportional to $\rho(r) \propto 1/r^2$. To find physical solutions, it is necessary to introduce a cut-off. The assumption in the King model is that a cluster cannot keep stars whose velocity exceeds a finite escape velocity. Therefore the velocity distribution should drop to zero at a finite limiting velocity. As a result, the cluster has a finite radius. Different cut-offs in the velocity distribution give different limiting radii. Observationally the finite boundary is set by the tidal forces of the galaxy with which the globular cluster is associated, which become dominant at a certain distance from the cluster center. The resulting velocity distributions are simply the Maxwell—Boltzmann distributions minus a constant. Let us assume the following form at the origin:

$$f(0,\vec{v}) = \begin{cases} \alpha\left(e^{-\frac{\beta v^2}{2}} - e^{-\frac{\beta v_e(0)^2}{2}}\right) & v \le v_e \\ 0 & v > v_e \end{cases} \tag{A7}$$

where α is a positive constant. This way the fastest particles $v > v_e(0)$ are subtracted from the distribution. The distribution of the velocities at $r = 0$ is defined by two parameters: β (which determines the width of the distribution) and $v_e(0)$, the escape velocity.

According to Jeans' theorem, any steady-state solution of the collisionless Boltzmann equation is a function of the integrals of motion (see for instance [28], p. 220). Since energy is the integral of motion in a star cluster the distribution function can be written as a function of the energy E:

$$f(\vec{r},\vec{v}) = f(E). \tag{A8}$$

We express the cut-off as an escape energy E_e such that $f = 0$ for $E \geq E_e$. The escape energy corresponds to an escape velocity at a point r through:

$$E_e = \frac{v_e(r)^2}{2} + V(r). \tag{A9}$$

$$f(E) = \begin{cases} \alpha\, e^{\beta(V(0)-E_e)}\left[e^{-\beta(E-E_e)} - 1\right], & E < E_e \\ \\ 0 & E \geq E_e. \end{cases} \tag{A10}$$

where α is a positive constant.

Substituting the distribution function into $(A2)$ and changing variables give us:

$$w \equiv \left(\frac{\beta}{2}\right)^{\frac{1}{2}} v \tag{A11}$$

$$\chi(r) \equiv \beta\,(E_e - V(r)) \tag{A12}$$

Thus we get

$$\rho = \begin{cases} 4\,\pi\,\alpha\, e^{-\chi(0)}\,(\frac{2}{\beta})^{\frac{3}{2}} I(\chi), & r < R_e \\ \\ 0 & r \geq R_e. \end{cases} \tag{A13}$$

where

$$I(x) \equiv \int_0^{\sqrt{x}} \left(e^{x-w^2} - 1\right) w^2\, dw, \tag{A14}$$

and R_e is the radius of the cluster such that $v_e(R_e) = 0$, and $\chi(R_e) = 0$. In other words, any star that succeeds in reaching R_e escapes the cluster and is no loner a part of the cluster.

When we substitute the density (A13) in the Poisson equation (A3) we get the fundamental equation of the King model

$$\frac{1}{\zeta^2}\frac{d}{d\zeta}\left(\zeta^2 \frac{d\chi}{d\zeta}\right) = -\frac{I(\chi)}{I(k)} \tag{A15}$$

with the boundary conditions

$$\chi(0) = k, \quad \chi'(0) = 0, \tag{A16}$$

where the rescaled dimensionless distance is

$$\zeta \equiv r(4\,\pi\, C\,\beta\,\rho(0))^{\frac{1}{2}}. \tag{A17}$$

The set of King solutions for the density is a one parameter family of solutions which are conveniently parameterized by k, the rescaled potential at the center.

Using the expression for the density (A13) and the fundamental equation (A15), we can write the mass in the following way:

$$M(r) = 4\,\pi \int_0^r \rho(r')\, r'^2\, dr' = \\ = -\,(4\,\pi\,\rho(0))^{-\frac{1}{2}}\ (\beta\, C)^{-\frac{3}{2}}\, \zeta^2 \chi'(\zeta). \tag{A18}$$

Note that here too, in the limit $k \to \infty$, the singular solution $(A4)$ is recovered (see [26]).

In Fig. 4 we give the average kinetic energy (per unit mass) as a function of R_s for various King solutions. The average kinetic energy (per unit mass) $\langle E_k \rangle$ is given by:

$$\langle E_k \rangle = \frac{1}{2}\langle v^2 \rangle = \frac{1}{2}\iint v^2\, f(\vec{r},\vec{v}) d^3\vec{r}\, d^3\vec{v}, \tag{A19}$$

when $f(\vec{r},\vec{v})$ is normalized so that

$$\iint v^2\, f(\vec{r},\vec{v}) d^3\vec{r}\, d^3\vec{v} = 1. \tag{A20}$$

In the case of an isotropic distribution of velocities and spherical symmetry we get:

$$v^2(r) = \int_0^{v_e(r)} v^4\, f(r,v)\, dv \Bigg/ \int_0^{v_e(r)} v^2\, f(r,v)\, dv\ . \tag{A21}$$

Substituting $(A10)$ and changing variables according to $(A11)$ and $(A12)$ we obtain:

$$v^2(r) = \frac{2}{\beta}\int_0^{\sqrt{\chi}} \left(e^{\chi - w^2} - 1\right) w^4\, dw\, /I(\chi) \tag{A22}$$

for $r < R_e$. Integration by parts gives us:

$$v^2(r) = \frac{6}{5\beta}\frac{J_6(\chi(r))}{J_4(\chi(r))}, \tag{A23}$$

where

$$J_n(x) \equiv \int_0^{\sqrt{x}} w^n\, e^{-w^2} dw. \tag{A24}$$

Repeating the steps in Eqs. $(A21)$-$(A23)$ with additional integration over the spatial directions gives the average kinetic energy:

$$\langle E_k \rangle = \frac{1}{2}\langle v^2 \rangle = \frac{3}{5\beta}\frac{\int_0^{R_e} r^2 dr\, e^{\chi(r)} J_6(\chi(r))}{\int_0^{R_e} r^2 dr\, e^{\chi(r)} J_4(\chi(r))}. \tag{A25}$$

In Fig. (4) $\langle v^2 \rangle$ is given for a series of solutions of Eq. (A15) with different values of k. For simplicity we take $\beta = 3/5$ in this figure.

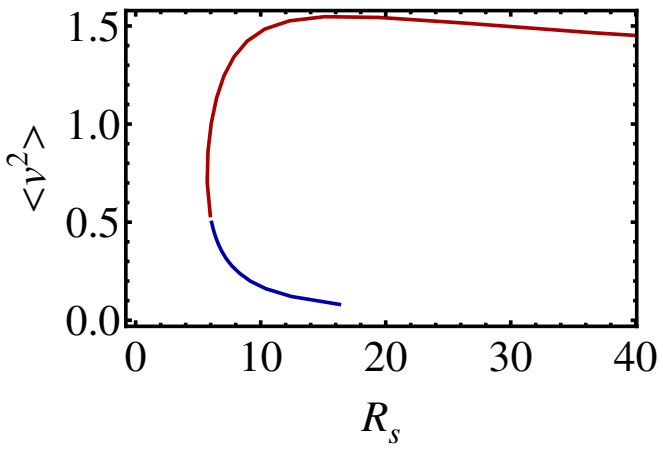

FIG. 4. The average kinetic energy (per particle) as a function of R_s for a series of King solutions. The blue and the red lines stand for the stable and unstable branches in the canonical ensemble respectively. Note that in the limit of large clusters the average kinetic energy is approximately independent of the cluster size.

The local velocity dispersion of a spherically symmetric distribution function is defined by [26]

$$\sigma^2(r) = \frac{v^2(r)}{3}. \tag{A26}$$

The average velocity is given by

$$\langle v \rangle = \frac{\int_0^{R_e} r^2\, dr \int_0^{v_e(r)} v^3\, f(r,v) dv}{\int_0^{R_e} r^2\, dr \int_0^{v_e(r)} v^2\, f(r,v) dv}, \tag{A27}$$

and then we can write the dispersion normalized by the average velocity:

$$\frac{\sigma(r)}{\langle v \rangle} = \frac{4}{3\sqrt{5}} \sqrt{\frac{J_6(\chi(r))}{J_4(\chi(r))}} \Bigg/ \frac{\int_0^{R_e} r^2 dr\, e^{\chi(r)}\, J_5(\chi(r))}{\int_0^{R_e} r^2 dr\, e^{\chi(r)} J_4(\chi(r))} \tag{A28}$$

Appendix B: The Time Evolution of the Swarm in the Simulation

Here we show a typical oscillatory behavior as a function of time of the half-mass radius (Fig. 5) and the size of the swarm (defined as the mean distance from the center of the swarm) in Fig. 6 for initial conditions that do not cause evaporation (over the time segment that is presented here). In Fig. 7, we show that the same swarm with different initial conditions evaporates over the same time segment (Fig. 7). Such cases were not considered as stable in this paper, and were ignored.

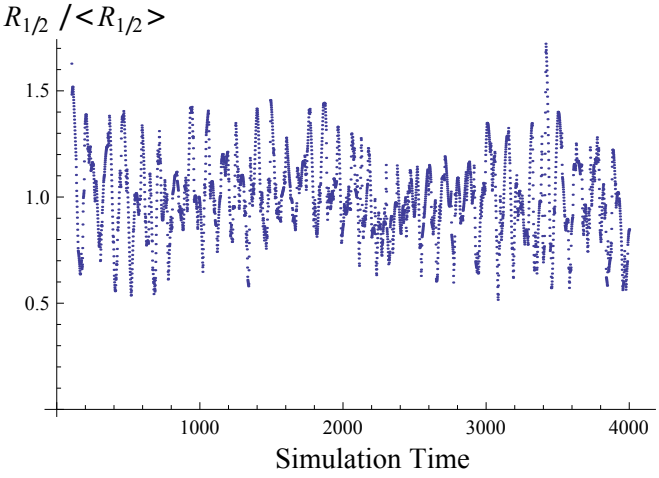

FIG. 5. The half-mass radius (normalized by its mean value) as a function of simulation time for a swarm with adaptivity ($R_{ad} = 5$) and 50 individuals. The half-mass radius is defined as the minimal radius that bounds half of the individuals in the swarm. Over the sampled time period the swarm seems to be stable for the randomly chosen initial conditions, which means that the evaporation takes place on a longer time scale.

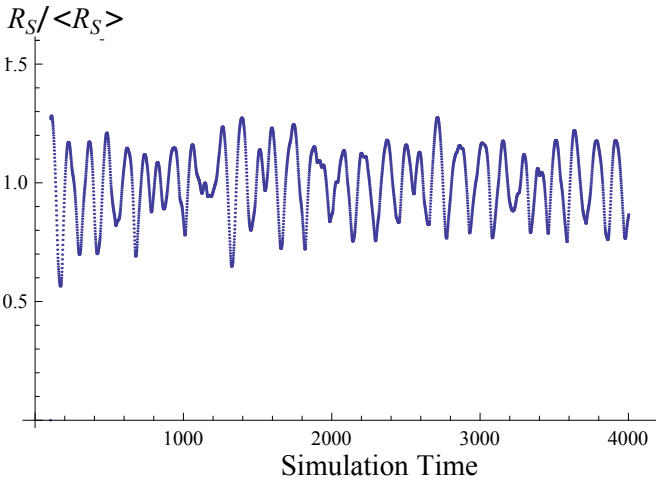

FIG. 6. The size of the swarm (normalized by its mean value) as a function of simulation time for the same swarm as in Fig. 5 ,where the size is defined as the mean distance from the center of the mass of the swarm.

Appendix C: The velocity and acceleration distributions

The distribution of a single component of the velocity in the simulation is given in Fig. 8 for various swarm sizes. In Fig. 9 we give the similar distribution of a single component of the acceleration. The structure of the tails is similar to the distributions that were obtained from the laboratory data [4].

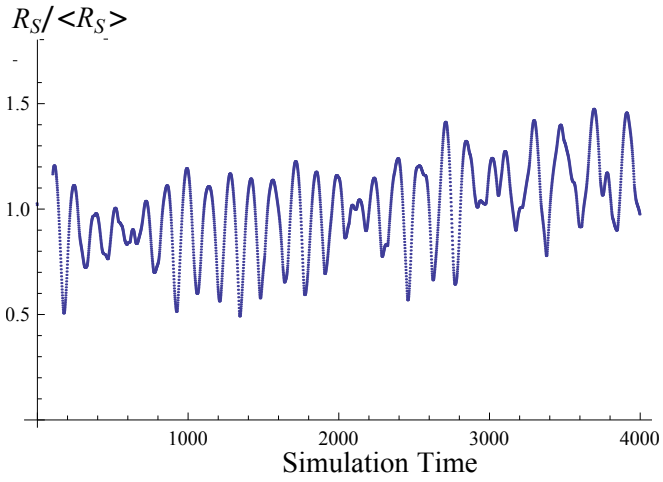

FIG. 7. The size of the swarm (normalized by its mean value) as a function of simulation time for a swarm with adaptivity ($R_{ad} = 5$) and 50 individuals. Here, in this example, different initial conditions lead to evaporation at earlier times than the previous example in Fig. 6. In the examples that we considered in this paper, we did not include time segments similar to this one that showed significant evaporation.

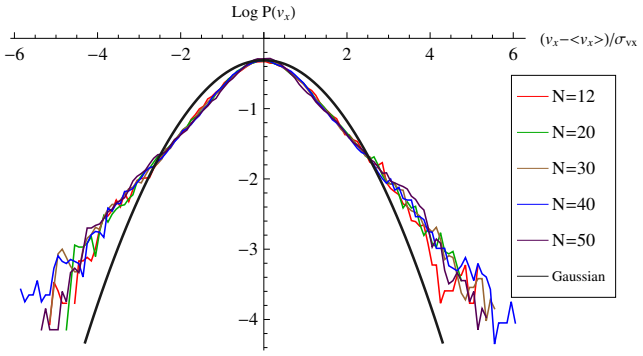

FIG. 8. The distribution of the x component of the velocity normalized by its standard deviation for different simulated swarms with adaptivity ($R_{ad} = 5$). A reference Gaussian curve is shown in black.

Appendix D: The relation between mean acceleration and speed

It was observed in [17] that if we take the mean acceleration of the right or left hemisphere of the swarm separately, its absolute value is a monotonically increasing function of the speed. The observational data from [17] for various sizes of swarms is reproduced here in Fig. 10d where the speed is normalized with respect to its mean value. Comparing with the simulation results (for ϵ-gravity in Fig. 10a, adaptivity in Fig. 10b and adaptivity with short-range repulsion in Fig. 10c) for swarms of different sizes, we see that in the cases with adaptivity (with and without repulsion) all the graphs collapse at

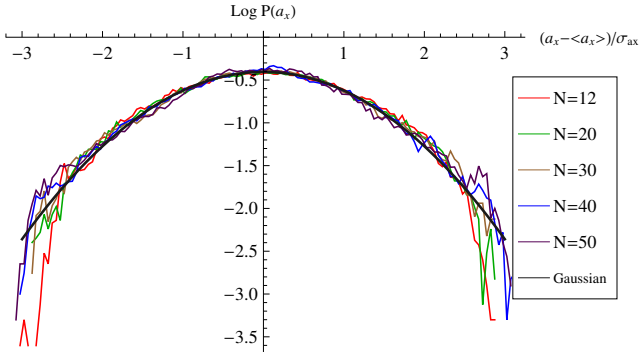

FIG. 9. The distribution of the x component of the acceleration normalized by its standard deviation for different simulated swarms with adaptivity ($R_{ad} = 5$). The acceleration distribution is bounded and cannot reach values that are too far from the average value. This is a result of the addition of the adaptivity and the softening parameter ϵ to the simulation, which are needed to slow down the evaporation of the swarm. A reference Gaussian curve is shown in black.

low velocities to have approximately the same acceleration, whereas in the ϵ-gravity case there are various values of acceleration at low velocities that do not agree with the observational data in Fig. 10d. One can also see that with repulsion there is more noise at high velocities. The agreement that we see here between adaptivity and the observational data suggests that adaptive gravity naturally explains the dependence of the acceleration on the mean velocity, without the need to invoke any additional explicit velocity-dependent forces [17].

Appendix E: The standard deviation of the speed in the simulations and the laboratory measurements

In addition to the uniformity of the average velocity across the midge swarm in the observational data (Fig. 3), we observe the same uniformity for the standard deviation of the speed (Fig. 11). The addition of adaptivity to the model recovers this behavior, as seen in Fig. 11.

In Fig. 12 we see the full range of velocity profiles and standard deviations of the speed for the simulations that include adaptivity and repulsion. For $r > 2\,R_s$ the velocities are found to increase to very high values and the density is very low. This region corresponds to particles that were expelled out of the swarm at high velocities due to the short-range repulsive interactions. We therefore do not consider this regime to be meaningful with respect to the properties of swarms.

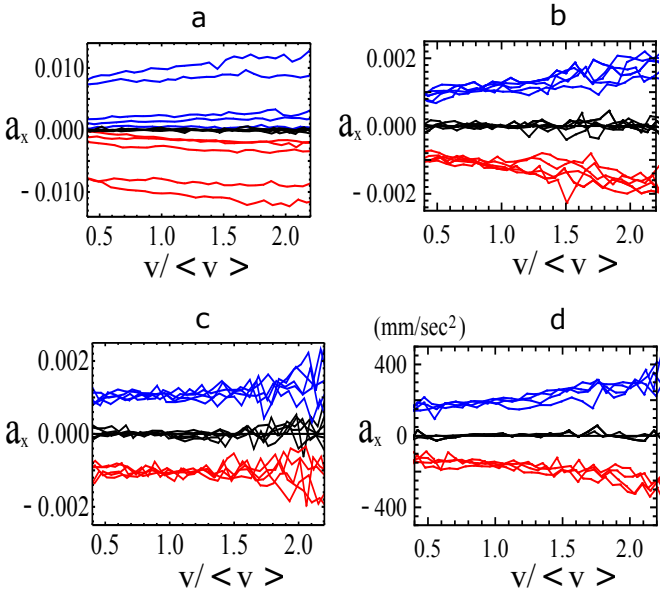

FIG. 10. The mean value of a single component of the acceleration versus the speed (normalized by the average speed) of the left hemisphere (blue), right hemisphere (red), and both hemispheres (black). The overall acceleration (black lines) is close to zero, as required by symmetry. Data are shown for (a) ϵ-gravity for different values of R_s (with $R_s = 16.23, 3.16, 19.53, 18.37, 30.10$ from top to bottom), (b) adaptive gravity, (c) adaptive gravity with repulsion, and (d) observational data.

Appendix F: Kinetic energy in the simulation

The kinetic energy of each midge in the laboratory measurements is approximately constant and does not depend on the density or the size of the swarm. In the simulations, since we are interested only in the mutual forces, we do not require constant speed for the particles, and therefore the kinetic energy per individual is different for various numbers of particles and initial conditions. We chose initial conditions that give us approximately the same kinetic energy per individual in the case of simulations with adaptivity and adaptivity with repulsion (within about 10%). Without adaptivity, we could not change significantly the kinetic energy by varying the initial conditions, and so it was determined mainly by the number of particles in the simulation.

Appendix G: The simulation with softened gravity ("epsilon-gravity")

In order to avoid high accelerations due to close encounters ("slingshots") and thus evaporation of the cluster, we included a softening parameter ϵ to the gravitational force (Eq. (1)). The particles in the simulation still developed high accelerations in close encounters relative to simulations with adaptivity since adaptivity itself contributed to the decrease of accelerations by $\epsilon^2/(R_{ad}^2+\epsilon^2)$,

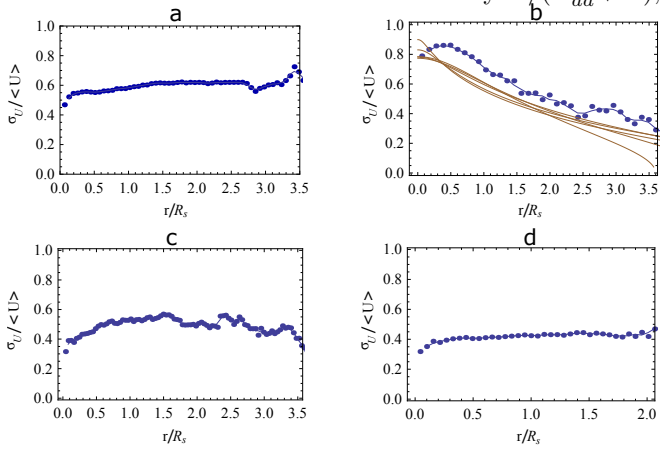

FIG. 11. The standard deviation of the speed (σ_U) normalized by the average speed in the swarm as a function of the distance from the center of mass normalized by the swarm size R_s. Data are shown for (a) laboratory observations, (b) simulation ofϵ-gravity (note that the brown curves correspond to a family of King solutions computed numerically according to Eq. ($A28$)), (c) adaptive gravity, and (d) adaptive gravity with repulsion.

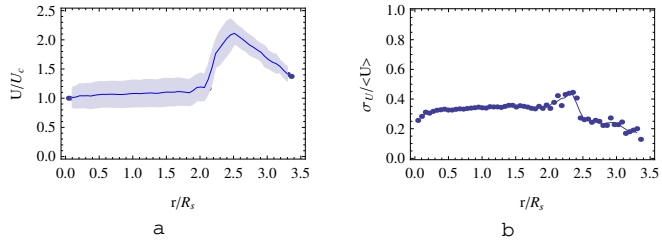

FIG. 12. (a) Mean speed (normalized by the speed at the swarm center) and (b) its standard deviation (normalized by the average speed) as functions of the distance from the swarm center for simulations with adaptvity and repulsion. For $r > 2\,R_s$, the velocities can become up to two times larger and the standard deviation can become two times lower. At the same time, the density is less than 10^{-5} of the density at the center (Fig. 1). Therefore, this regime likely describes particles that were repelled out of the swarm at high velocities (higher than the escape velocity).

and in order to compare the simulations in the two cases (with and without adaptivity) we have to reduce the accelerations in the "ϵ-gravity" case by this constant factor. The results in Fig. 15 were obtained in this way. In Fig. 15(a) density profiles for various sizes of clusters are given (where $\epsilon^2 = 15$) and in Fig. 15(b)-(d) we show three characteristic quantities of the clusters: the number of particles, the density at the center and the kurtosis. Here and throughout the paper we truncated the tails at $r \sim 3\,R_s$ in the calculation of the kurtosis.

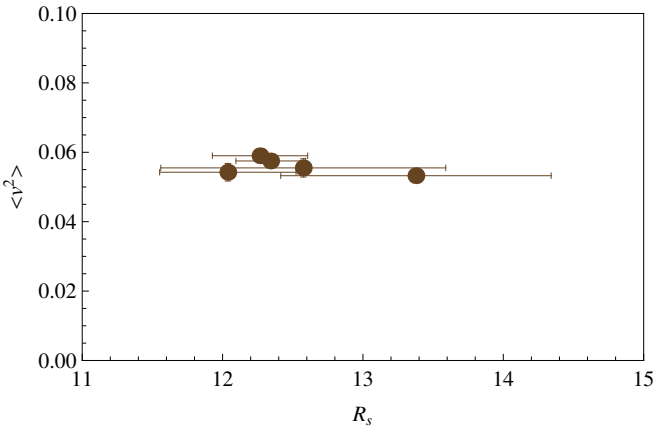

FIG. 13. The kinetic energy as a function of the size of the swarm R_s for cases with adaptivity (Fig. 2). Here the size of the swarm does not change much but the number of individuals changes from 12 to 48 (Fig. 2).

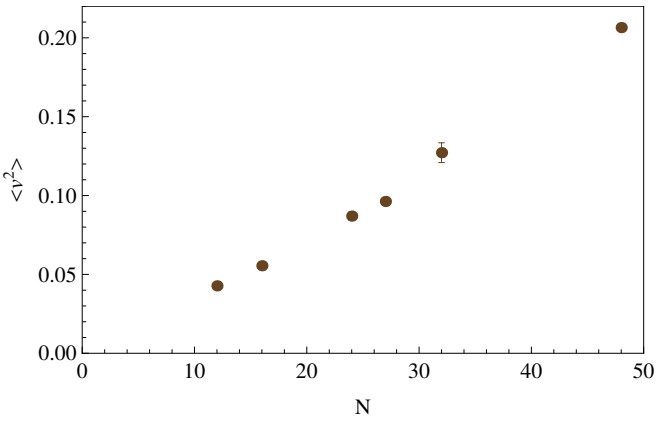

FIG. 14. The kinetic energy as a function of the number of individuals N in the simulation for the cases without adaptivity (Fig. 15).

[1] J. Krause and G. D. Ruxton, *Living in Groups* (Oxford University Press, Oxford, 2002).
[2] D. Sumpter, *Collective Animal Behavior* (Princeton University Press, Princeton, 2010).
[3] A. Okubo, Adv. Biophys. **22**, 1 (1986).
[4] D. H. Kelley and N. T. Ouellette, Sci. Rep. **3**, 1073 (2013).
[5] A. Attanasi, A. Cavagna, L. Del Castillo, I. Giardina, S. Melillo, L. Parisi, O. Pohl, B. Rossaro, E. Shen, E. Silvestri, and M. Viale, Phys. Rev. Lett. **113**, 238102 (2014).
[6] R. Ni, J. G. Puckett, E. R. Dufresne, and N. T. Ouellette, Phys. Rev. Lett. **115**, 118104 (2015).
[7] M. Sinhuber, K. van der Vaart, and N. T. Ouellette, J. R. Soc. Interface **16**, 20180739 (2019).
[8] K. van der Vaart, M. Sinhuber, A. M. Reynolds, and N. T. Ouellette, Science advances **5**, eaaw9305 (2019).
[9] A. Aldersley, A. Champneys, M. Homer, N. W. Bode, and D. Robert, Current Biology **27**, R1208 (2017).
[10] D. Gorbonos, R. Ianconescu, J. G. Puckett, R. Ni, N. T. Ouellette, and N. S. Gov, New J. Phys. **18**, 073042 (2016).
[11] D. Gorbonos and N. S. Gov, Phys. Rev. E **95**, 042405 (2017).
[12] J. Seuer, E. J. Tuck, and D. Robert, J. Acoust. Soc. Am. **118**, 530 (2005).
[13] T. Vicsek, A. Czirók, E. Ben-Jacob, I. Cohen, and O. Shochet, Phys. Rev. Lett. **75**, 1226 (1995).
[14] I. King, Astron. J. **71**, 64 (1966).
[15] P.-H. Chavanis, M. Lemou, and F. Méhats, Phys. Rev. D **91**, 063531 (2015).
[16] J. G. Puckett and N. T. Ouellette, Journal of The Royal Society Interface **11**, 20140710 (2014).
[17] A. M. Reynolds, M. Sinhuber, and N. T. Ouellette, Eur. Phys. J. E **40**, 46 (2017).

[18] M. Sinhuber, K. van der Vaart, R. Ni, J. G. Puckett, D. H. Kelley, and N. T. Ouellette, Sci. Data (2019).
[19] S. J. Aarseth, in *Multiple Time Scales*, edited by J. U. Brackbill and B. I. Cohen (Academic Press, Orlando, 1985).
[20] O. Shoval, L. Goentoro, Y. Hart, A. Mayo, E. Sontag, and U. Alon, Proc. Natl. Acad. Sci. USA **107**, 15995 (2010).
[21] J. G. Puckett, D. H. Kelley, and N. T. Ouellette, Scientific reports **4**, 4766 (2014).
[22] J. Binney and S. Tremaine, *Galactic Dynamics* (Princeton University Press, Princeton, 2011).
[23] A. M. Reynolds and N. T. Ouellette, Sci. Rep. **6**, 30515 (2016).
[24] A. M. Reynolds, Physical biology **16**, 046002 (2019).
[25] I. King, Astron. J. **71**, 64 (1966).
[26] P.-H. Chavanis, M. Lemou, and F. Méhats, Phys. Rev. D **91**, 063531 (2015).
[27] T. Padmanabhan, *Theoretical Astrophysics: Volume 1, Astrophysical Processes* (Cambridge University Press, 2000).
[28] J. Binney and S. Tremaine, *Galactic dynamics* (Princeton university press, 2011).

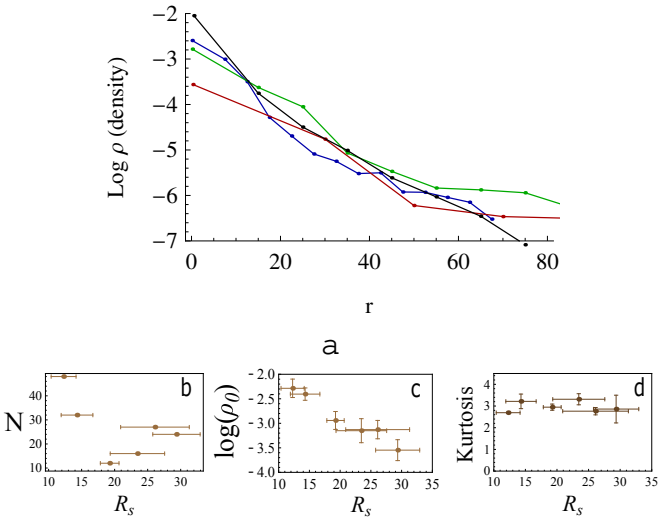

FIG. 15. (a) Density profiles of simulated clusters with the softened-gravity ("epsilon gravity") model. Data are shown for cases with $N = 48$, $R_s = 9.29$ (black); $N = 27$, $R_s = 26.08$ (green); $N = 16$, $R_s = 30$ (red); and $N = 12$, $R_s = 16.4$ (blue). (b)-(d) The total number of midges, the density at the center, and the kurtosis as functions of the size of the swarm for the "epsilon gravity" model (using $\epsilon^2 = 15$).